Weather and Climate Extremes 53 (2026) 100915

Contents lists available at ScienceDirect

Weather and Climate Extremes

journal homepage: www.elsevier.com/locate/wace

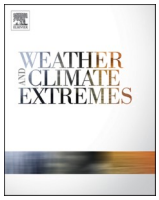

Climatology and trends of annual maximum subdaily precipitation in the Western United States

Dmitri A. Kalashnikov [a,*], John T. Abatzoglou [b], Daniel L. Swain [c,d]

[a] Sierra Nevada Research Institute, University of California, Merced, Merced, CA, USA
[b] College of Engineering, University of California, Merced, Merced, CA, USA
[c] California Institute for Water Resources, University of California Agriculture and Natural Resources, Davis, CA, USA
[d] Weather Extremes Across Scales Section, NSF National Center for Atmospheric Research, Boulder, CO, USA

A B S T R A C T

Short-duration precipitation extremes can threaten public safety and infrastructure by generating flash flooding and geophysical mass wasting events including mudslides and debris flows. Using two surface gauge-based precipitation datasets (1980-2024), we characterize the climatology of annual maximum subdaily precipitation and quantify trends across the western United States (WUS) – a topographically complex region with widely varying precipitation regimes prone to flash flooding. We find that 60.7% of WUS stations, including the vast majority of those located in the continental interior, typically experience 1-hr annual maximum precipitation (AMP) during summer and during the afternoon and evening hours (12:00-23:00 local time). Although most stations do not show statistically significant trends in 1-hr AMP intensity over the full period of record (1980-2024), a significant 10.3% domain-median increase in 1-hr AMP intensity was observed during 2000-2024. These changes largely result from seasonal maximum precipitation (SMP) increases during summer over the continental interior coinciding with a trend toward more favorable summer thermodynamic environments for short-duration precipitation extremes. We also report widespread though statistically insignificant increases in SMP intensity during winter and spring in California since 2000 coinciding with increased column water vapor. These results are suggestive of potential recent intensification of subdaily precipitation extremes in a warming climate in the WUS despite a backdrop of considerable internal variability.

1. Introduction

Short-duration precipitation extremes (occurring on time scales shorter than one day, hereafter 'subdaily') pose societal risks due to associated impacts from rapid inundation (i.e., flash flooding) and geophysical mass wasting events (e.g., mudslides, debris flows, and other slope failures), and are responsible for a majority of flood-related deaths in the United States (Ashley and Ashley, 2008; Brooks and Stensrud, 2000; James and Schumacher, 2024; Smith et al., 2018). The western United States (WUS) is a region of complex topography and varied precipitation regimes (Mock, 1996; Ralph et al., 2014). In the interior WUS, summertime thunderstorms associated with the North American Monsoon (NAM) produce some of the highest incidences of flash flooding in the nation due to the combination of heavy subdaily rainfall falling on steep terrain (Ahmadalipour and Moradkhani, 2019; Maddox et al., 1980; Papalexiou et al., 2018; Smith et al., 2019). Meanwhile, in the Pacific Coast states of Washington, Oregon, and California, intense subdaily precipitation is most common during the winter wet season. A particularly destructive recent example of the risk posed by such extremes occurred on 9 January, 2018, in Montecito, California, when ~26 mm (>1 inch) of rain in 15 min generated debris flows that killed 23 people and destroyed hundreds of structures (Oakley et al., 2018). This event occurred in very steep topography recently burned by a large wildfire, thereby amplifying runoff and illustrating an increasing compound hazard in an era of escalating wildfire activity (Thomas et al., 2024; Touma et al., 2022). Despite their potentially outsized impacts, subdaily precipitation events have been understudied for practical reasons including limitations in the availability of hourly data compared to daily data and challenges in obtaining, processing, and quality-controlling hourly precipitation data from surface weather stations (Lewis et al., 2019, 2021; Pritchard et al., 2023).

Our study is further motivated by recent extreme subdaily precipitation events observed in the WUS. In California, for instance, ~81 mm (3.18 inches) of rain fell in 1 h in Oxnard on 21 December, 2023, while more than >50 mm (>2 inches) fell in 3 h in San Diego on 22 January, 2024, with both events causing significant urban flooding, necessitating swiftwater rescues, and representing the greatest precipitation on record at those durations for each observation site (Center for Western Weather and Water Extremes, 2024; Graff, 2023). Farther inland, the NAM was active in 2021 and 2022 with numerous instances of heavy convective rainfall and flash flooding across the Southwest that damaged roads and forced closures of national parks (Horel and Powell, 2024; National Park

* Corresponding author. Sierra Nevada Research Institute, University of California, Merced, Merced, CA, USA.
E-mail address: dkalashnikov@ucmerced.edu (D.A. Kalashnikov).

https://doi.org/10.1016/j.wace.2026.100915
Received 25 November 2025; Received in revised form 18 May 2026; Accepted 19 May 2026
Available online 20 May 2026

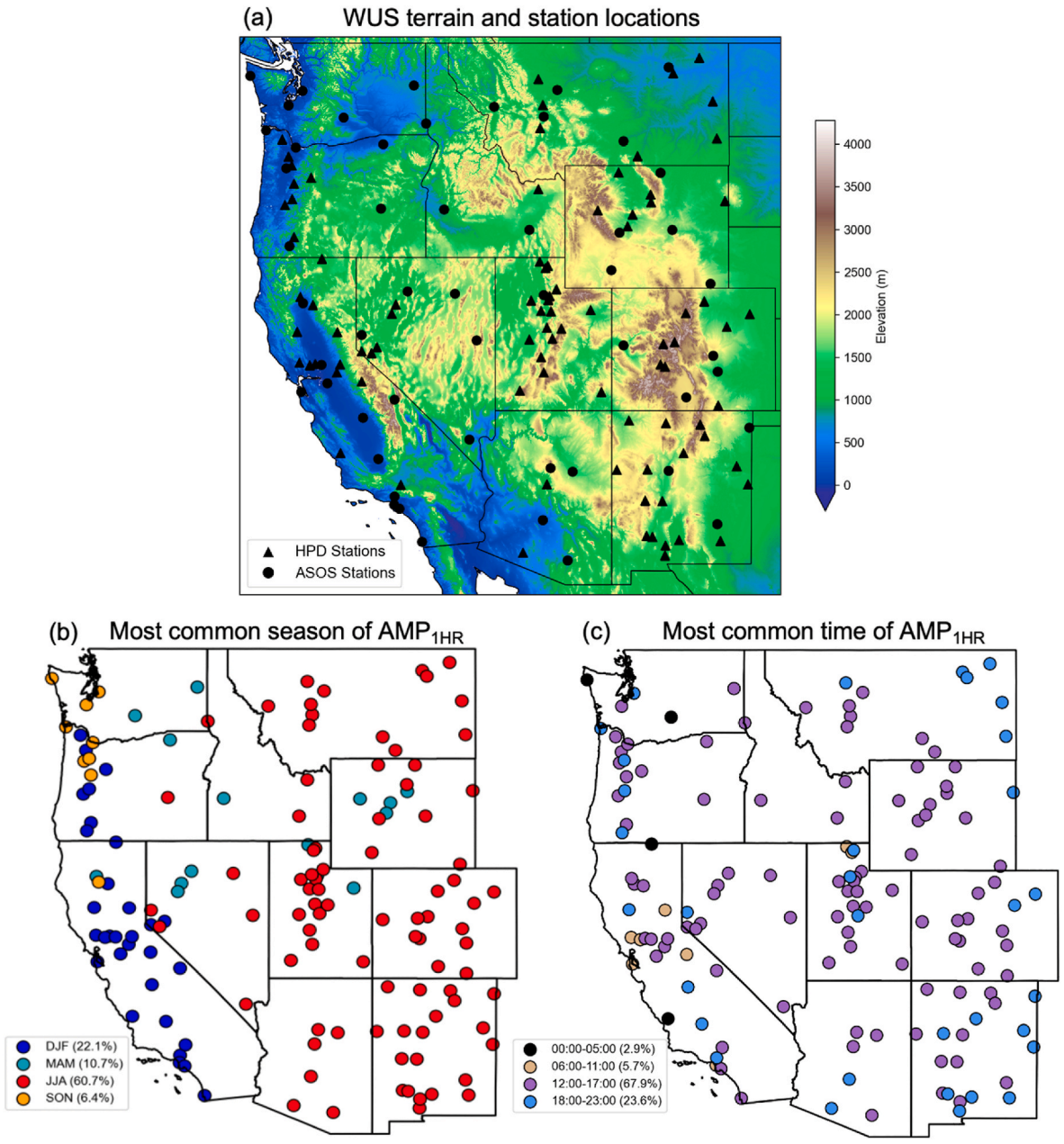

Fig. 1. (a) WUS terrain elevation with station locations denoted by black markers. Most common (b) season and (c) time of day of AMP_{1HR} events during 1980-2024, with percent of stations represented by that bin shown in the legend.

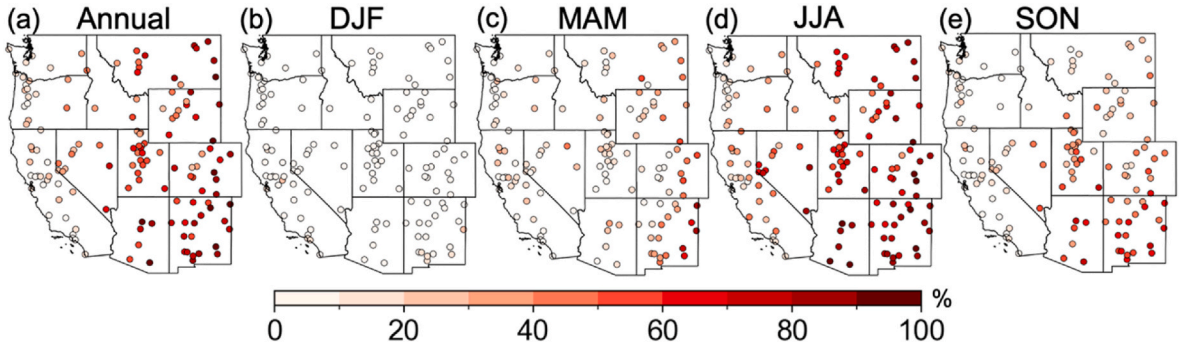

Fig. 2. Percent of annual maximum 1-hr precipitation events associated with cloud-to-ground (CG) lightning during 1995-2024 (a) annually (AMP_{1HR}) and (b-e) over the four calendar seasons (SMP_{1HR}).

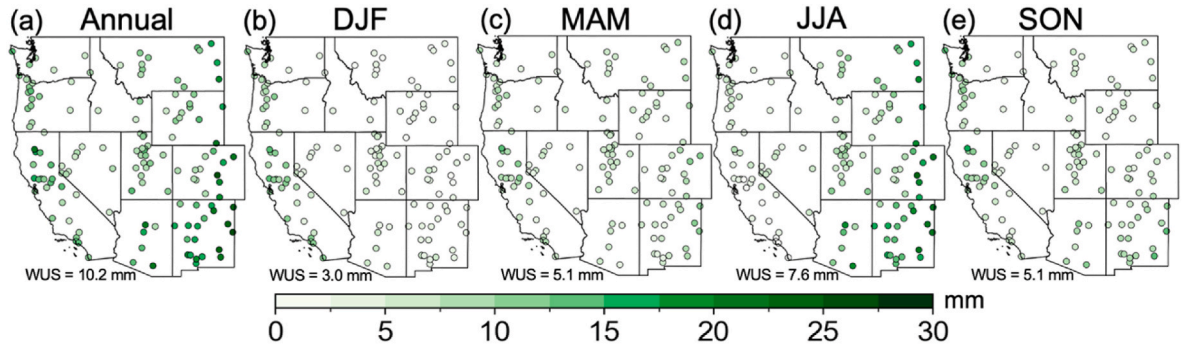

Fig. 3. Median annual/seasonal maximum 1-hr precipitation amounts during 1980-2024 (a) annually (AMP_{1HR}) and (b-e) over the four calendar seasons (SMP_{1HR}). Inset text shows domain median amounts.

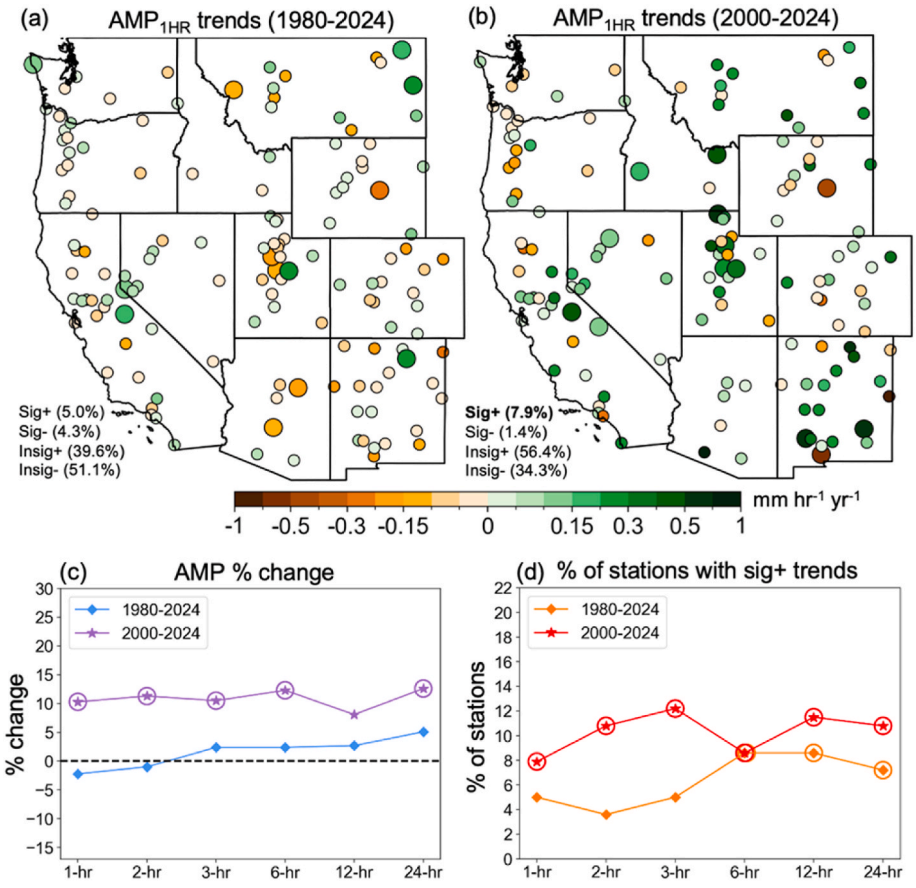

Fig. 4. Linear trends in AMP_{1HR} intensity over (a) 1980-2024 and (b) 2000-2024. Large circles indicate that trends are statistically significant ($p < 0.10$) according to a two-tailed *t*-test. Inset text shows the percent of stations with significant positive (sig+), significant negative (sig-), insignificant positive (insig+) and insignificant negative (insig-) trends. For significant trends, bolded values indicate field significance over the domain based on a resampling procedure (see Fig. S1 for the resampled distributions). (c) Domain-median percent change in AMP intensity at different subdaily aggregations on an annual basis. Circled datapoints indicate that AMP changes are significant based on a resampling procedure. (d) As in (c), but showing percent of stations with sig + trends in AMP intensity at different subdaily aggregations. Circled datapoints indicate that positive trends are field-significant.

Service, 2022; National Weather Service, 2023). While observed trends in annual maximum precipitation intensity at the daily scale show limited changes to date across the WUS (Williams et al., 2024), here we consider how annual maximum subdaily precipitation intensity has changed across this region.

Climate change is expected to intensify subdaily precipitation extremes primarily due to the increased capacity of warmer air to hold additional water vapor as described by the Clausius-Clapeyron (C-C) relation (Allen and Ingram, 2002; Fowler et al., 2021; Trenberth et al., 2003). Despite this well-established relationship, the response of extreme subdaily precipitation to warming can vary widely between regions and across precipitation-generating processes due to confounding influences from changes to near-surface aridity, atmospheric dynamics, and small-scale convective processes. Indeed, recent studies have shown a stronger response of precipitation extremes to near-surface moisture changes (e.g., dewpoint temperature or relative humidity) than temperature changes alone (Barbero et al., 2018; Cannon et al., 2024; Lenderink et al., 2017; van der Drift and O'Gorman, 2025); potential shifts in the frequency of large-scale atmospheric patterns or other dynamical changes (thereby affecting moisture

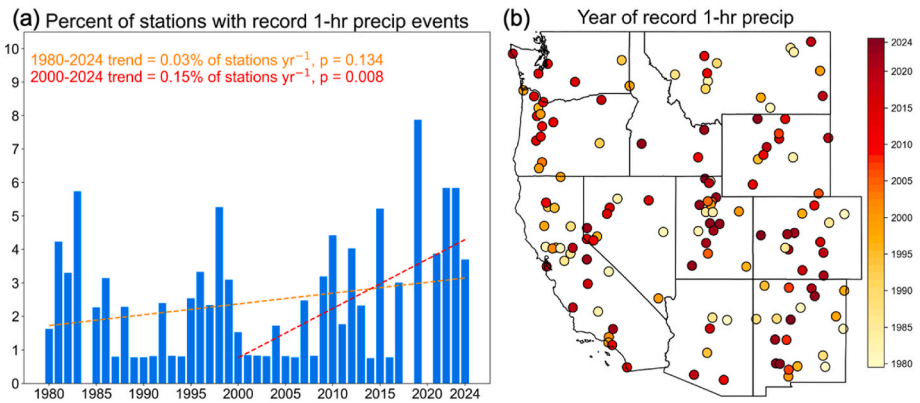

Fig. 5. (a) Percent of stations each year with period-of-record maximum 1-hr precipitation events, representing the maximum observed values at each station over 1980-2024 (i.e., "all-time" records). For example, in 2019, 10 of the 127 available stations (~7.9%) recorded their "all-time" record 1-hr precipitation (Table 1). Linear trends in the annual percent of stations with period-of-record maximum 1-hr precipitation events are shown for 1980-2024 (orange) and 2000-2024 (red) with p-values from two-tailed *t*-test. (b) Year of period-of-record maximum 1-hr precipitation. In cases of ties from multiple years in (a) and (b), the year of latest occurrence is considered.

Table 1
Stations that observed their annual period-of-record (among all available years between 1980 and 2024) maximum 1-hr precipitation in 2019. Records are listed in chronological order.

Station	Date of record	Time of record (local)	Amount (mm)	Amount (inches)
Paso Robles, CA	17 JAN 2019	00:00	25	1.00
PUB Airport (Pueblo, CO)	17 JUN 2019	14:53	41	1.61
Bredette, MT	27 JUN 2019	05:00	41	1.60
Ekalaka, MT	8 JUL 2019	20:00	41	1.60
Logan 5SW Experimental Farm, UT	27 JUL 2019	01:00	23	0.90
Ajo, AZ	31 JUL 2019	14:00	56	2.20
Newcastle, WY	10 AUG 2019	17:00	58	2.30
Boysen Dam, WY	11 SEP 2019	12:00	20	0.80
UIL Airport (Quillayute, WA)	21 OCT 2019	14:53	28	1.10
Fiddletown Dexter Ranch, CA	7 DEC 2019	18:00	38	1.50

convergence) could also affect trends in subdaily precipitation extremes (e.g., Dallan et al., 2024).

In addition, subdaily precipitation extremes may also increase at a greater rate than pure C-C scaling (+7% per °C of warming) might otherwise suggest – perhaps by a factor of two or more due to invigorated convective processes (Ali et al., 2021; Fowler et al., 2021; Huang et al., 2020; Lenderink et al., 2017; Li and Li, 2023). Extreme subdaily precipitation, therefore, offers a compelling target for further investigation as it might simultaneously be expected to exhibit accelerated intensification and pose disproportionately increased societal risks relative to extreme daily precipitation in a warming climate.

In this study, we use quality-controlled station data from two observational networks to quantify the climatology and examine changes in the intensity of annual maximum subdaily precipitation over the WUS during 1980-2024. Our approach aims to fill several existing research gaps. For example, recent studies that have examined subdaily extreme precipitation over this region have typically used only one observational network (e.g., Barbero et al., 2017; Mascaro et al., 2025), leaving uncertainties due to observational practices and limited geographic coverage of available stations. Our study offers an update to Barbero et al. (2017), who did not report meaningful trends in hourly precipitation intensity using data through 2011, and complements Mascaro et al. (2025), who reported a recent emerging trend in the frequency of subdaily heavy precipitation in the United States using data through 2020, but did not quantify changes in intensity. Here, we quantify trends in the intensity of the annual maximum precipitation (AMP) as well as seasonal maximum precipitation (SMP) at multiple subdaily to daily aggregations (1, 2, 3, 6, 12, and 24-hr) through 2024 to understand recent observed changes. To better understand the physical processes driving these changes, we also examine trends in the thermodynamic environments associated with subdaily precipitation extremes across the WUS. Although we conduct our analyses at multiple subdaily aggregations, we pay particular attention to hourly precipitation extremes given the established links between hourly precipitation and flash flooding (Brooks and Stensrud, 2000; James and Schumacher, 2024).

2. Data and methods

2.1. Precipitation datasets

We use hourly precipitation data from two observational networks to improve the geographic coverage of available stations – the Automated Surface Observing System (ASOS) network that serves airports and is typically located in larger population centers, and the Cooperative Observer Program Hourly Precipitation Data version 2 (COOP-HPD v2, hereafter 'HPD') that is more widely distributed in urban to rural areas. ASOS precipitation data were sourced from the Iowa Environmental Mesonet (https://mesonet.agron.iastate.edu/request/download.phtml), while the HPD data were sourced from the National Centers for Environmental Information (NCEI) (https://www.ncei.noaa.gov/access/metadata/landing-page/bin/iso?id=gov.noaa.ncdc:C00988). Both datasets are subset to the 11 states wholly contained within the conterminous WUS. Although hourly precipitation observations at some stations extend to the early to middle 20th century, we restrict our analyses to the 1980-present period due to widespread adoption of tipping bucket gauges and a larger pool of available stations after the 1970s (Wallis et al., 2007). This results in an initial pool of 656 ASOS stations and 537 HPD stations of varying data quality, completeness, and length of observational record. Extensive quality control (QC) procedures and selection criteria are applied to both datasets to ensure a homogenized and consistent record among the stations and are described below.

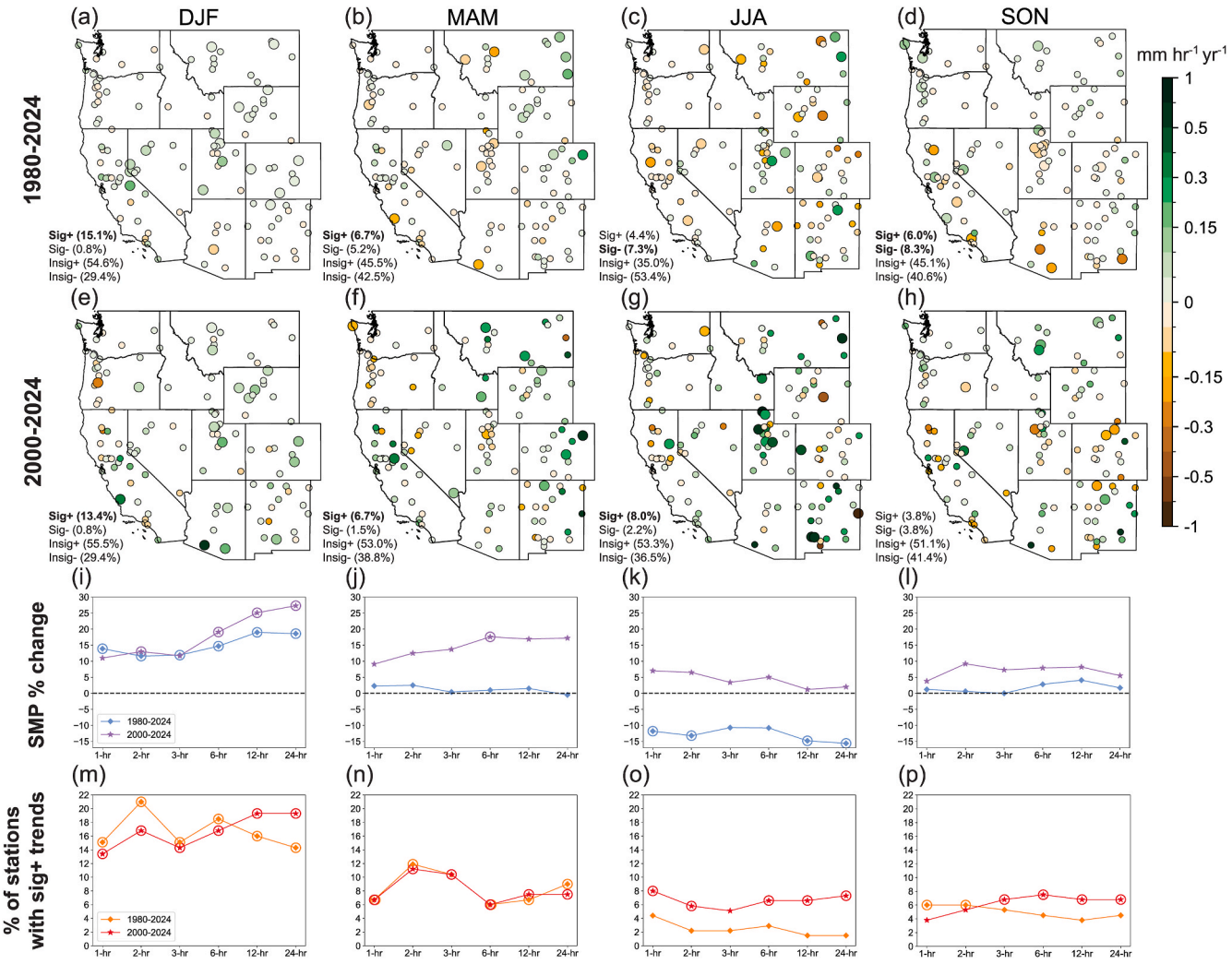

Fig. 6. Linear trends in intensity during (a-d) 1980-2024 and (e-h) 2000-2024 as in Fig. 4a–b, but for SMP_{1HR} over the four calendar seasons. (i-p) As in Fig. 4c–d, but for the four calendar seasons.

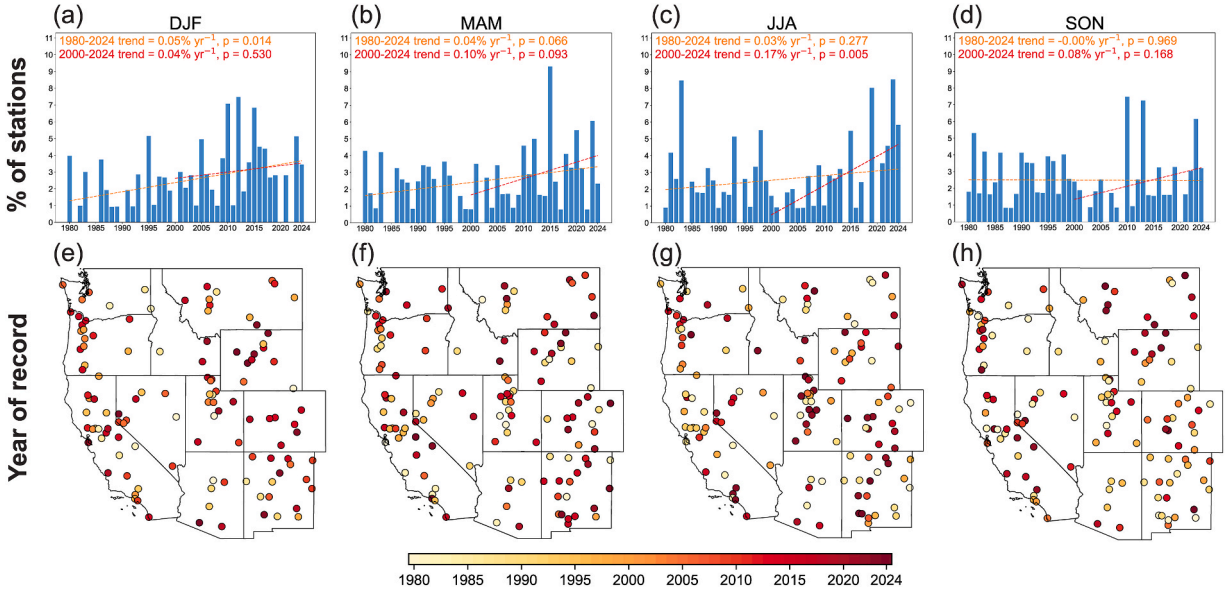

Fig. 7. (a-d) Percent of stations each year with period-of-record maximum 1-hr precipitation events and (e-h) year of record 1-hr precipitation as in Fig. 5, but for the four calendar seasons. See Table 2 for a list of stations that observed their period-of-record JJA maximum 1-hr precipitation in 2023.

Table 2
Stations that observed their JJA period-of-record (among all available years between 1980 and 2024) maximum 1-hr precipitation in 2023. Records are listed in chronological order.

Station	Date of record	Time of record (local)	Amount (mm)	Amount (inches)
Ocate 2NW, NM	6 JUN 2023	13:00	48	1.90
Grantsville 2W, UT	31 JUL 2023	15:00	30	1.20
Nephi, UT	2 AUG 2023	13:00	28	1.10
Scofield Skyline Mine, UT	2 AUG 2023	14:00	30	1.20
Powell Field Station, WY	7 AUG 2023	14:00	20	0.80
Cedar City 5E, UT	18 AUG 2023	16:00	33	1.30
Palmdale, CA	20 AUG 2023	08:00	18	0.70
BUR Airport (Burbank, CA)	20 AUG 2023	18:53	9	0.34
LGB Airport (Long Beach, CA)	20 AUG 2023	23:53	8	0.33
BOI Airport (Boise, ID)	22 AUG 2023	17:53	19	0.73
Echo Dam, UT	23 AUG 2023	19:00	25	1.00

2.2. Preprocessing and quality control

First, HPD data already contain some level of preprocessing and quality control (Lawrimore et al., 2020). We thus remove any HPD hourly observations that contain QC flags or are marked as missing. A unique challenge to the HPD dataset is the changing measurement precision over time, wherein many stations recorded precipitation at 2.54 mm (0.10 inch) resolution over the late 20th to beginning of the 21st century before converting to 0.254 mm (0.01 inch) resolution in recent decades (Lawrimore et al., 2020). To ensure temporal consistency of hourly observations, all HPD stations were converted to the coarser 2.54 mm resolution prior to analysis following Groisman et al. (2012).

Potential missing observations in ASOS are denoted by an 'M' flag. However, the accuracy and consistency of this flag is undocumented across the network's observational record, and some instances of missing observations simply recorded as zero were suspected. We therefore treat all instances of zero or 'M' as potential missing values and apply Tukey's interquartile range (IQR) method to flag and exclude station years with an unrealistically small number of wet hours (precipitation $\geq$0.254 mm) (Tukey, 1977). For each station, the annual counts of wet hours are first summed to form a distribution. The first (Q1) and third (Q3) quartiles are calculated as well as the IQR (Q3 – Q1). The lower bound ($Bound_{lower}$) for inclusion is computed as follows:

$$Bound_{lower} = Q1 - (1.5 * IQR)$$

wherein any station years that have summed wet hours below the $Bound_{lower}$ are considered incomplete and excluded. By excluding years at ASOS stations with a large amount of missing precipitation data, this step also handles stations that did not consistently measure precipitation in the earlier part of their record but may have routinely observed other meteorological parameters critical for aviation (e.g., temperature, pressure, and wind) and would therefore not be flagged in later completeness checks.

The following QC and selection steps are conducted across both networks. We exclude all years with >20% missing data and select only currently active stations as of 2024. This step enforces a robust sample size within each year, a common ending year among all stations for consistent interpretation of trends across the domain, and recency. Further, we retain only stations with $\geq$80% of years that have $\geq$80% data completeness (i.e., at least 36 of the 45 years between 1980 and 2024). These criteria are stringent and necessarily result in many excluded stations, and other studies that examined subdaily precipitation trends applied more relaxed constraints to increase sample size. For example, Barbero et al. (2017) allowed the ending year to vary between 2000 and 2011 for stations in their analysis, rather than enforcing a recent common ending year. However, this creates a potentially undesirable scenario wherein trends at some stations could be outdated by more than a decade at the time of reporting. Meanwhile, both Barbero et al. (2017) and Mascaro et al. (2025) allowed for much shorter available data coverage at individual stations than the nominal analysis period. In the case of the former, the analysis period spanned 1950-2011 but individual stations needed only >30 years of observations to be included; while in the latter study, the analysis period spanned 1949-2020 but only required 40 years of observations at individual stations. Although such approaches increase the spatial coverage of stations and may improve the robustness of trend detection, the potentially large differences in available years among stations confounds interpretation of long-term trends.

We also remove stations with inhomogeneous observations over the period of record, which could stem from factors including changes to measurement practices or equipment, station moves, and vegetation encroachment (Court, 1960; Groisman and Legates, 1994). Inhomogeneities are flagged using the Pettitt test that identifies changepoints in the time series of annual-total precipitation at each station (Pettitt, 1979), consistent with prior studies examining precipitation extremes (e.g., Barbero et al., 2017). We note that statistically significant changepoints may also reflect genuine hydroclimatic non-stationarity; however, this criterion resulted in the exclusion of only five stations from the analysis.

Finally, a check of selected extreme station-level hourly precipitation amounts identified the presence of potentially spurious values in the ASOS network that were recorded during dry and stable atmospheric patterns. To control for this, we compare hourly precipitation amounts at each station across both networks to their corresponding daily, quality-controlled precipitation totals from the Global Historical Climatology Network daily (GHCNd) dataset, sourced from the NCEI (https://www.ncei.noaa.gov/products/land-based-station/global-historical-climatology-network-daily). Any hourly amounts that exceed the daily-total precipitation are flagged and removed. For HPD stations, the following day is also checked as daily COOP station observations typically overlap two calendar days. For ASOS stations, the corresponding GHCNd stations represent the same locations and measuring equipment and are compared directly. When comparing HPD stations, an important caveat is that GHCNd data are collected from co-located but separate daily rainfall gauges and may be subject to different data availability over the period of record compared to the hourly HPD gauges (Lawrimore et al., 2020). We therefore exclude any HPD stations that do not have a corresponding GHCNd station subject to the same constraints of $\geq$80% available years with $\geq$80% data completeness and active in 2024. Overall, the QC process yielded a final pool of 140 stations that are retained for analysis, including 88 HPD and 52 ASOS stations (Fig. 1a).

2.3. Trend assessment

Employing a block maxima approach, we compute linear trends in AMP and SMP intensity (one data point per year over 1980-2024) at each station for each subdaily aggregation between 1 and 24-hr and assess trend significance ($p < 0.10$) using a two-tailed *t*-test. Intensity at different subdaily aggregations is denoted by subscripts (e.g., AMP_{1HR} for 1-hr AMP, AMP_{2HR} for 2-hr AMP) and represents annual-maximum values in rolling windows of that length. Trends and test statistics are calculated using only the available years at each station. We also assess trends over 2000-2024 to test whether increases in AMP and SMP intensity exist over the recent period.

When conducting multiple hypothesis testing, a certain percentage

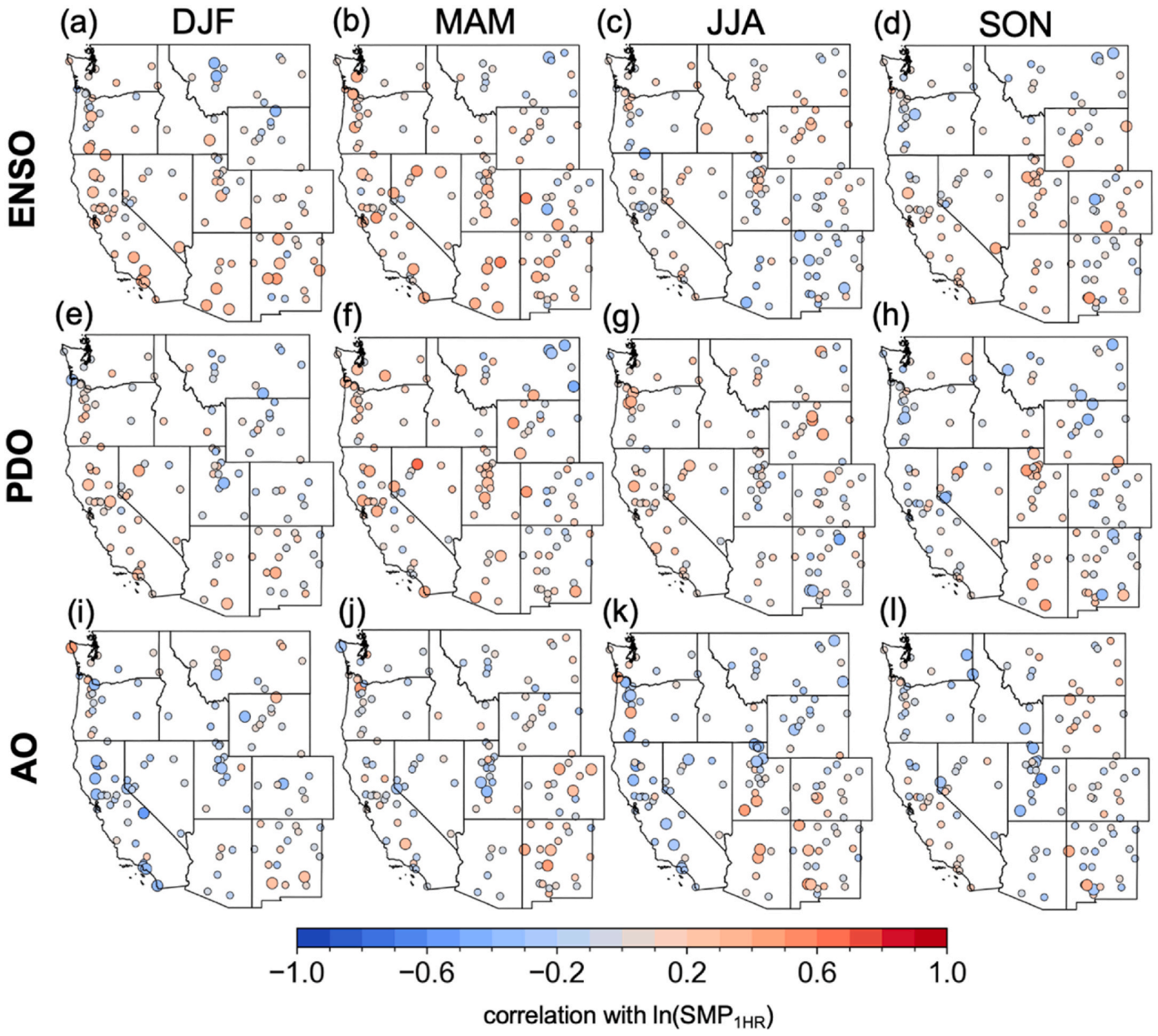

Fig. 8. Pearson's correlation between the natural logarithm of SMP_{1HR} amounts ($ln(SMP_{1HR})$) and seasonally-averaged indices of ENSO, PDO, and AO. Large circles indicate statistical significance ($p < 0.10$).

of stations can contain significant trends due to random chance. To ensure robustness of our findings, we compute field significance for both the number of significant positive and negative AMP and SMP intensity trends across the domain using a resampling-based procedure (Barbero et al., 2017; Westra et al., 2013). First, an m x n matrix is constructed with m rows representing the years and n columns representing the station-level AMP or SMP values, and the rows are then randomly shuffled 100 times. This procedure randomizes the time series while preserving the spatial structure of station-level precipitation data (Westra et al., 2013). Although this reshuffling procedure does not preserve potential temporal autocorrelation, AMP and SMP timeseries consist of temporally sparse block maxima for which serial correlation is expected to be relatively weak. For each of the 100 iterations, the percent of stations with significant positive and negative trends is computed to form the randomized trend distribution. Second, we also control for the possibility that the observed percent of stations with significant trends could arise due to the random placement of stations across space. This is done by randomly subsetting 50% of the stations 100 times and computing their trend distributions following Barbero et al. (2017). To determine field significance of trends, we compare these spatially resampled observational distributions with the temporally randomized distributions from the first step using a Mann-Whitney U test ($p < 0.10$; Fig. S1). Finally, we conduct bootstrap resampling ($n = 1\,000$ replicates) to determine significance of domain-median AMP and SMP intensity changes over the period of record, computed from the percentage changes at individual stations. Domain-median intensity changes are deemed significant if the observed change lies outside of the 90% confidence interval of the resamples.

We conduct trend analyses for both AMP and for SMP intensity over the four canonical seasons: December-January-February (DJF), March-April-May (MAM), June-July-August (JJA), and September-October-November (SON). For both AMP and SMP analyses, we restrict the assessment of trends and correlations (Section 2.4) to stations with ≤ 3 ties in their period-of-record maximum 1-hr precipitation. This is done

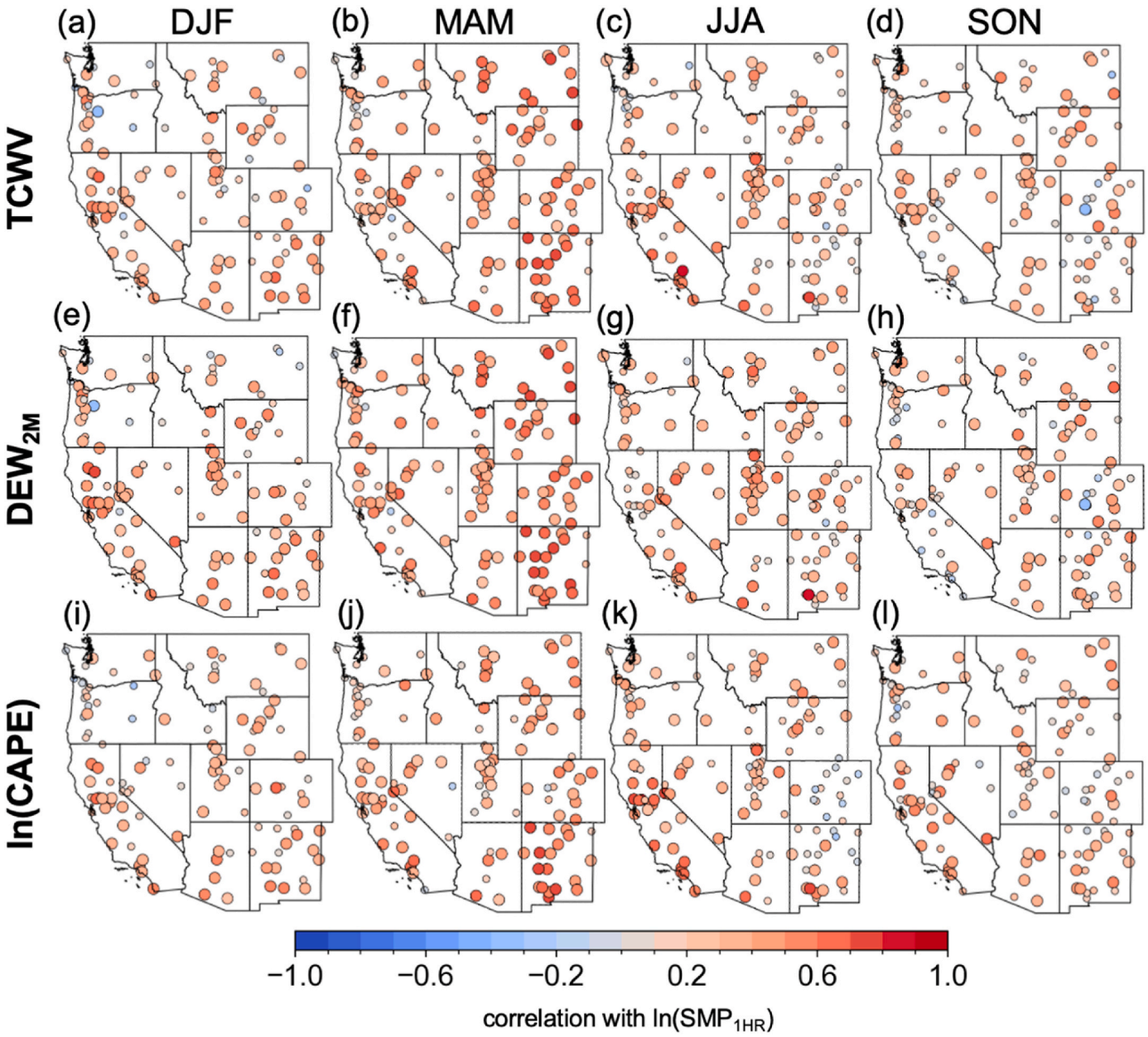

Fig. 9. Pearson's correlation between the natural logarithm of SMP_{1HR} amounts ($\ln(SMP_{1HR})$) and daily averages of total column water vapor (TCWV), 2-m dewpoint (DEW_{2M}), and the natural logarithm of Convective Available Potential Energy (ln(CAPE)) on AMP_{1HR} days. Large circles indicate statistical significance ($p < 0.10$).

to exclude HPD stations in dry regions and during dry seasons that may have numerous ties at low values from multiple years due to the 2.54 mm (0.10 inch) precision, which could complicate trend assessment. As a result, the number of retained stations for the analysis of trends and correlations is 139 for the annual scale, 119 for DJF, 134 for MAM, 137 for JJA, and 133 for SON.

To complement the analysis of station-level trends, we compute the number of stations experiencing period-of-record, or "all-time record," maximum subdaily precipitation in each year, similar to prior work that quantified trends in the number of all-time temperature records across the United States (Abatzoglou and Barbero, 2014). In cases of ties, we retain the most recent occurrence of the all-time record at each station. To account for annual variability in the number of stations with complete data, we normalize the number of stations with record subdaily precipitation in a given year by the number of reporting stations that year. We then calculate and report linear trends in the percent of stations reporting all-time records across years.

2.4. Meteorological and climate variables

Meteorological variables are sourced from the European Centre for Medium-Range Weather Forecasts (ECMWF) ERA5 reanalysis at 0.25° resolution (Hersbach et al., 2020). These variables include total column water vapor (TCWV), 2-m dewpoint (DEW_{2M}), and convective available potential energy (CAPE). We conduct two analyses to understand the relationships between these variables and subdaily precipitation extremes at each station. First, we compute Pearson's correlation between daily-mean values of these variables and AMP (or SMP) intensity. We apply a natural log transformation to both CAPE and precipitation amounts to treat nonnormality in the raw distributions. Second, we compute standardized anomalies (z-scores) of the variables on AMP (or SMP) days using 15-day centered windows over 1980-2024. We then test for significant difference of the positive anomalies from zero using a one-tailed t-test. Finally, we calculate trends in these variables over 1980-2024 and 2000-2024 to quantify changes in thermodynamic

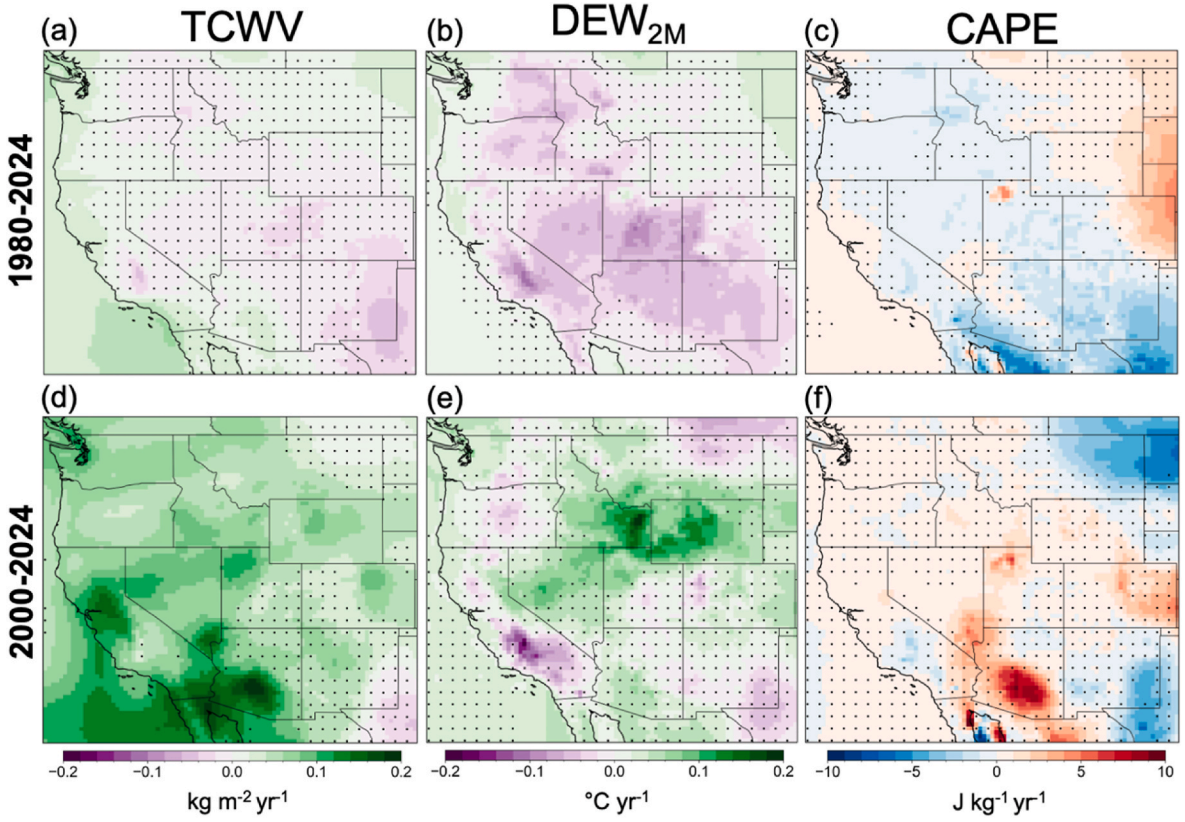

Fig. 10. Linear trends in JJA season-mean TCWV, DEW_{2M}, and CAPE over (a-c) 1980-2024 and (d-f) 2000-2024. Stippling shows insignificant grid cells ($p \geq 0.10$; two-tailed *t*-test).

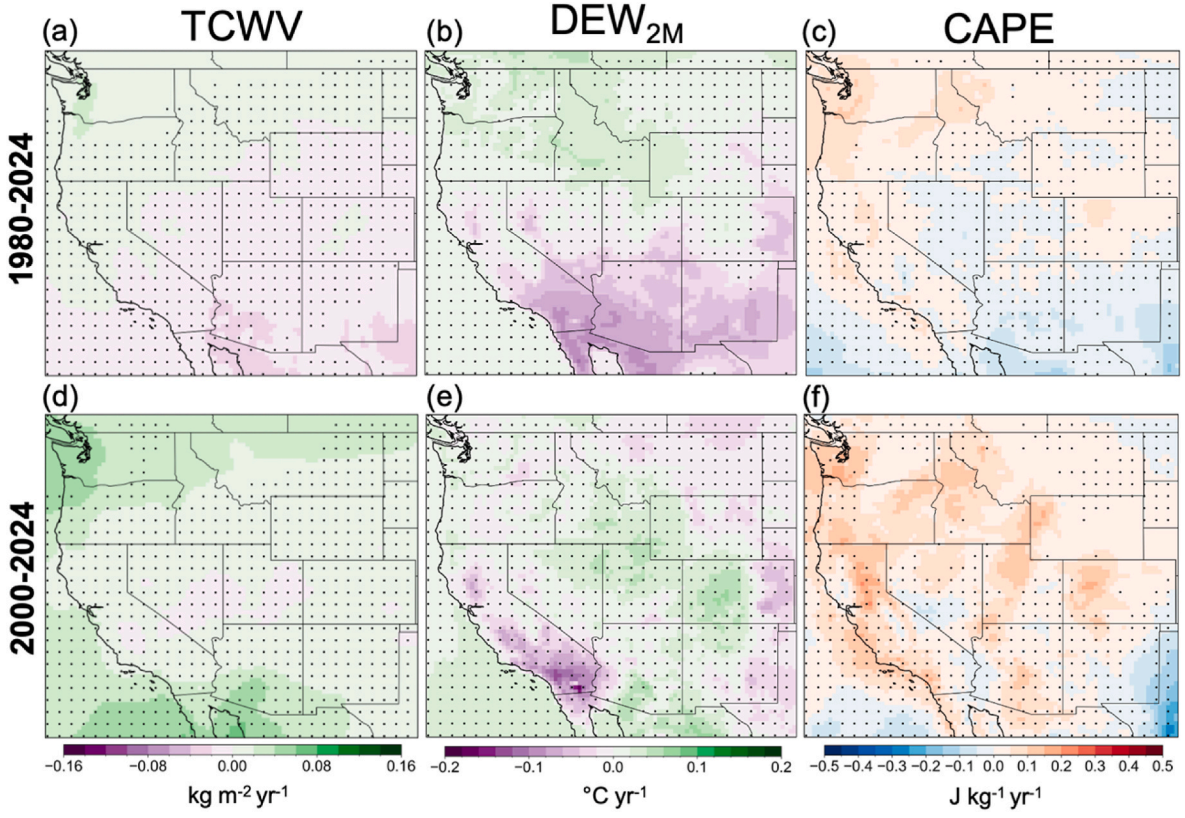

Fig. 11. Linear trends as in Fig. 10, but for DJF.

environments that may affect subdaily precipitation extremes. To capture overall background conditions and reduce noise in the trend analysis, we use season-mean values of these variables. Linear trends are computed and assessed for significance using a two-tailed *t*-test. Results of all statistical testing are deemed significant at $p < 0.10$.

To associate subdaily precipitation extremes with cloud-to-ground (CG) lightning, we use daily CG lightning data from the National Lightning Detection Network (NLDN) at $0.1^\circ \times 0.1^\circ$ spatial resolution that was extracted from the grid cell overlying each station. Although NLDN data extends to the 1980s, we only use data from 1995-present as this follows a major sensor upgrade in 1994-95 that improved detection performance (e.g., Cummins and Murphy, 2009). We tabulate the percent of AMP and SMP events at each station that had ≥1 CG strike on the day coincident to the precipitation extreme.

We also analyze Pearson's correlation between SMP_{1HR} intensity during all four seasons and several modes of large-scale climate variability. These include the El Niño-Southern Oscillation (ENSO), the Pacific Decadal Oscillation (PDO), and the Arctic Oscillation (AO). To quantify ENSO conditions, we use the Relative Oceanic Niño Index (RONI) over the Niño 3.4 region (5°N-5°S, 120°-170°W). RONI and AO were sourced from the Climate Prediction Center (CPC), while PDO data were sourced from the National Centers for Environmental Information (NCEI). Correlation results are deemed significant at $p < 0.10$.

3. Results and discussion

3.1. Climatology of 1-hr annual maximum precipitation

We find that at 60.7% of WUS stations, AMP_{1HR} events occur most commonly during JJA (Fig. 1b). This includes the vast majority (86.6%) of stations in the continental interior (i.e., the WUS excluding the three coastal states) where the terrain is largely elevated and summertime convection, often driven by the NAM, is common. At a further 22.1% of stations, AMP_{1HR} events typically occur during DJF mostly located in the coastal states of California and Oregon, where DJF accounts for 76.3% of AMP_{1HR} events. Near-coastal environments in these states experience a Mediterranean climate characterized by wet winters and mostly dry summers. Only 17.1% of stations typically observe AMP_{1HR} events during MAM and SON combined, primarily in Washington and scattered locations from the northern Great Basin into the central Rockies. AMP_{1HR} events occur most commonly during the afternoon and evening (12:00-23:00 local time) at 91.5% of WUS stations (67.9% during 12:00-5:00) including nearly all stations in the interior WUS, reflecting the predominantly deep moist convective character of these precipitation events as instability and thunderstorm activity are maximized during afternoon heating (Fig. 1c). Indeed, the majority of JJA SMP_{1HR} and consequently AMP_{1HR} events across the interior WUS occur in conjunction with cloud-to-ground lightning (Fig. 2).

Median AMP_{1HR} amounts vary substantially across the domain, with a domain-median of 10.2 mm (Fig. 3a). Higher amounts >25 mm are found in areas along the east-facing slopes of the Rocky Mountain Front Range where moisture-rich air from the Gulf of Mexico can be advected especially during JJA (Fig. 3d). However, elevated values > 20 mm are also present in parts of Arizona and western New Mexico, where intense thunderstorm downpours associated with the NAM can occur during summer months (Fig. 3d) (Adams and Comrie, 1997; Barlow et al., 1998). Meanwhile, lower AMP_{1HR} amounts occur in the arid continental interior away from the NAM core (Fig. 3a). We note that the sparse (or even absent) sampling due to lack of long-term hourly observation sites of acceptable quality in locations including the Coast Ranges and California's Sierra Nevada and Transverse Ranges likely misses the high DJF SMP_{1HR} and AMP_{1HR} values that likely occur in these regions during cool-season atmospheric river storms (Fig. 3a–b) (e.g., Huang et al., 2020).

3.2. Annual and seasonal trends in subdaily precipitation intensity

AMP_{1HR} intensity shows generally mixed trends for the full 1980-2024 period, with slightly more than half of the stations (55.4%) observing decreases in intensity and a lack of field significance for either significant positive (5% of stations) or negative (4.3% of stations) trends (Fig. 4a, S1). However, field-significant positive trends are present during 2000-2024, with 7.9% of stations observing statistically significant increases in intensity against only 1.4% with statistically significant decreases, with 64.3% of stations observing overall increases in AMP_{1HR} intensity (Fig. 4b). Results from a Mann-Kendall nonparametric trend test are similar, with the fraction of stations reporting significant increasing trends during 2000-2024 (6.4%) substantially outpacing those with significant decreasing trends (2.9%) (Fig. S2). Meanwhile, domain-median AMP_{1HR} intensity declined by 2.2% during 1980-2024 but increased by 10.3% during 2000-2024 ($p < 0.10$; Fig. 4c). The presence of field-significant positive trends since 2000 is even more apparent for AMP_{2HR} and AMP_{3HR} extremes, which showed field-significant decreases (at 8.6% and 6.5% of stations, respectively) during 1980-2024 but field-significant increases (at 10.8% and 12.2% of stations, respectively) during 2000-2024 (Fig. 4d–S3, S4a). Increases are especially pronounced in the interior Southwest where most station-level significant increases are located, similar to the results of Mascaro et al. (2025), as well as across parts of California.

The annual fraction of stations, calculated from all available stations that year, experiencing their period-of-record maximum 1-hr precipitation (i.e., either breaking or tying their "all-time" records) has increased significantly since 2000 (+0.15% of stations yr^{-1}; $p = 0.008$), substantially outpacing the overall trend since 1980 (+0.03% of stations yr^{-1}; $p = 0.134$) (Fig. 5a). Notably, the three individual years in which the largest fraction of stations experienced period-of-record maximum 1-hr precipitation have all occurred during the most recent decade – 2019, 2022, and 2023 – with 10 stations experiencing records in 2019 alone (Table 1). Increases in the annual fraction of stations experiencing period-of-record maximum subdaily precipitation since 2000 are apparent for 2-hr and 3-hr aggregations as well (Fig. S3c and f). Spatially, most of the recent station-level records have occurred in the Four Corners region of Arizona, New Mexico, Utah, and Colorado that typically experience AMP events during JJA (Fig. 5b). In this region, a notably large fraction of stations (43.1%) observed absolute 1-hr records during 2015-2024. This is in contrast to the Northwest, where very few period-of-record maximum 1-hr precipitation events occurred in the recent decade.

At the seasonal scale, DJF and MAM show field-significant positive trends in SMP intensity at all subdaily aggregations between 1-hr and 24-hr during both 1980-2024 and 2000-2024 (Fig. 6). The strongest signal is during DJF, with 15.1% of stations observing significant increases in SMP_{1HR} intensity during 1980-2024 reducing slightly to 13.4% during 2000-2024, in agreement with Barbero et al. (2017) who found widespread increases in SMP_{1HR} intensity during winter. Between 13.4% and 21% of stations contain significant DJF positive trends for all subdaily aggregations over both analysis periods, with domain-median intensity increases of between 11 and 27% (Fig. 6i–m, S5).

By contrast, the coastal states of California, Oregon, and Washington are largely devoid of statistically significant SMP_{1HR} increases in DJF and MAM during 2000-2024. This could be because cool-season dynamics have counteracted anthropogenic forcing by reducing moisture transport to the region (Williams et al., 2024), particularly over the Northwest, or simply that statistically robust subdaily precipitation trends have not yet emerged from the noise of background climate variability (Kendon et al., 2023; McKinnon and Deser, 2021; Wood and Ludwig, 2020). Nevertheless, a majority of California stations show statistically insignificant positive intensity trends during DJF and MAM during both 1980-2024 and 2000-2024 (Fig. 6). Notable increases are apparent during 2000-2024 in MAM when 79.2% of stations show positive trends, resulting in a state-median 26.3% increase in SMP_{1HR}

intensity (compared to an 8.2% increase over the full 1980-2024 period). In the interior WUS, significant positive trends are present at 18.4% of stations in DJF and 8.8% in MAM during 2000-2024. However, cool-season SMP increases in these states are not expected to meaningfully influence AMP trends (Fig. 4), as affected stations are located in areas where AMP events typically occur during JJA.

Meanwhile, a marked difference in trends is apparent during JJA between 1980-2024 and 2000-2024 with widespread increases over the most recent period. Whereas only 39.4% of stations contain increases overall since 1980 for SMP_{1HR} intensity, positive trends are present at 61.3% of stations during 2000-2024 (Fig. 6c–g). The sign of field significance has also changed from negative for 1980-2024 to positive for 2000-2024, with 8% of stations observing significant increases over the latter period. Similar trend differences between the two periods are observed for other JJA subdaily aggregations (Fig. 6o–S6). Likewise, although JJA SMP intensity decreases of 11-16% are observed for all subdaily aggregations during 1980-2024 (significant for 1, 2, 12, and 24-hr durations), insignificant increases are apparent for all aggregations during 2000-2024 including a 7% increase in SMP_{1HR} intensity (Fig. 6k). Moreover, stations with significant JJA increases since 2000 are concentrated in the interior WUS where AMP events typically occur during this season (e.g., at 86.6% of stations; Fig. 1b). We therefore conclude that the presence of positive JJA SMP_{1HR} intensity trends since 2000, and mainly in the interior states, is largely driving the observed increases in WUS AMP_{1HR} intensity this century (Fig. 4). The JJA fraction of stations experiencing period-of-record maximum 1-hr precipitation has also increased significantly since 2000 (+0.17% of stations yr^{-1}; $p = 0.005$), in contrast to other seasons that do not show such robust increases, and recent station-level records are concentrated in the Four Corners region (Fig. 7c–g). Notably, 11 stations experienced period-of-record JJA maximum 1-hr precipitation in 2023 (Table 2), which included several stations in the Southwest directly affected by the remnants of Hurricane Hilary that dissipated on 20 August (Reinhart, 2024).

3.3. Relationship of SMP_{1HR} with climate variability modes

SMP_{1HR} intensity is significantly positively correlated with ENSO at many stations in the Southwest during DJF and MAM (Fig. 8a–b), likely reflecting canonical ENSO teleconnections during cool-season months in this region (National Weather Service, 2026). Across the domain, SMP_{1HR} intensity at >70% of stations is positively correlated with ENSO during both seasons. These findings reiterate that the established relationship between El Niño events and wetter seasonal conditions across the Southwest also extends to daily-to-hourly precipitation extremes (Li et al., 2020; Patricola et al., 2020). SMP_{1HR} intensity also shows widespread positive correlation with the PDO during MAM (69.4% of stations), with a notable exception in eastern Montana where significant negative correlations are present (Fig. 8f). Meanwhile, SMP_{1HR} intensity is negatively correlated with the AO at >60% of stations during both DJF and JJA, with negative correlations particularly prevalent in California (Fig. 8i–k). These findings are in agreement with prior work linking -AO conditions with more frequent and intense atmospheric rivers over the WUS that are in turn responsible for the majority of cool-season extreme precipitation events in this region (Huang et al., 2020; Liner et al., 2022; McCabe-Glynn et al., 2016).

3.4. Trends in thermodynamic environments

SMP_{1HR} intensity is significantly positively correlated with the three analyzed thermodynamic variables that represent atmospheric moisture content and vertical stability – TCWV, DEW_{2M}, and CAPE – at most WUS stations across the four calendar seasons (Fig. 9). These relationships are particularly strong across the Rocky Mountains and adjacent High Plains during MAM (Fig. 9b–f,j). Furthermore, across the vast majority of stations and seasons, the standardized anomalies (*z*-scores) of these variables are significantly elevated relative to climatology on SMP_{1HR} days (Fig. S7).

We assess changes in these variables to explore potential thermodynamic causes of observed trends in subdaily precipitation intensity. As the largest intensification in SMP_{1HR} events since 2000 has occurred during JJA (Fig. 6k), we mainly focus on changes to meteorological variables during this season. We find that all three variables show overall trends toward less favorable thermodynamic environments across the WUS in JJA during the full 1980-2024 period, with broad significant decreases ($p < 0.10$) in DEW_{2M} and CAPE (Fig. 10a–c). However, widespread significant TCWV increases and some regional increases in DEW_{2M} and CAPE in the interior WUS are apparent since 2000 (Fig. 10d–f). Meanwhile, widespread though statistically insignificant positive trends in TCWV are present during DJF and MAM over California since 2000 (Fig. 11d, S8d), aligning with general SMP_{1HR} increases over the state during these seasons (Fig. 6e–f), and are also present during SON (Fig. S9d). Widespread but insignificant positive CAPE trends are also present over California during DJF since 2000 (Fig. 11f).

While TCWV increases during JJA since 2000 align with thermodynamic expectations due to a warming atmosphere, the reasons for a lack of significant increases during the full 1980-2024 period are less obvious and may reflect low-frequency climate variability related to ENSO and PDO. For example, paleoclimate reconstructions have shown that the late 20th century was an anomalously wet epoch in the WUS (Cook et al., 2025) partially due to the persistence of positive ENSO and PDO conditions and regional-scale atmospheric circulation patterns favorable for increased precipitation (Bass et al., 2022), and this period was immediately followed by a severe multi-decadal "megadrought" (Williams et al., 2022) – both of which were of unprecedented magnitude in the last millennium. Given this exceptionally large regional swing from pluvial to drought over the late 20th to early 21st centuries, an apparent drying trend might be expected for a multi-decadal period of record beginning around 1980 even against the background of anthropogenically-forced atmospheric moisture increases at a global scale.

Meanwhile, decreases in near-surface absolute moisture – represented by DEW_{2M} – since 1980 agree with previously reported aridification of the Southwest in the past four decades (Simpson et al., 2024). However, the partial rebound in near-surface moisture availability across the interior WUS during JJA may represent a contributing factor to the increased SMP intensity this century, particularly given the previously reported scaling of extreme precipitation with dewpoint temperatures (Barbero et al., 2018; Cannon et al., 2024). Overall, evidence suggests that more favorable thermodynamic environments since 2000 during JJA may have contributed to an intensification of full-year AMP extremes this century, particularly in the interior WUS.

4. Summary and conclusions

4.1. Summary

In this study, we utilized two quality-controlled hourly precipitation datasets spanning 1980-2024 to quantify the climatology and trends in the intensity of subdaily precipitation events across the WUS, a topographically complex region that is prone to flash flooding, debris flows, and other geophysical mass wasting events. We pay particular attention to AMP_{1HR} and SMP_{1HR} events given the established links between 1-hr precipitation and flash flooding in mountainous and desert watersheds of the Southwest (James and Schumacher, 2024).

AMP_{1HR} events typically occur during JJA at 60.7% of WUS stations, including at 86.6% of stations in the interior states, with a lesser WUS fraction in DJF (22.1% of stations; primarily in California and western Oregon) and in MAM/SON (combined 17.1% of stations; primarily in the Northwest), and most commonly occur during the afternoon and evening hours (12:00-23:00) at 91.5% of stations (Fig. 1). The majority

of AMP_{1HR} events and JJA SMP_{1HR} events are associated with CG lightning in the eastern half of the domain in areas commonly affected by monsoonal convection during summer months (Fig. 2).

We find that although AMP_{1HR} intensity declined at a majority of stations during the full 1980-2024 period, a domain-median, significant intensification of 10.3% is apparent during 2000-2024 (Fig. 4). Further, field-significant positive trends in AMP intensity are detected at all subdaily aggregations from 1 to 24 h since 2000. These findings broadly align with Mascaro et al. (2025), who detected emerging trends in the frequency of subdaily precipitation extremes since 2000 across the United States. Notably, we also find that the percentage of stations experiencing period-of-record maximum 1-hr precipitation has increased across the WUS in recent decades, with apparent clustering in the Four Corners region (i.e., Arizona, New Mexico, Utah, and Colorado) where 43.1% of stations have observed their 1-hr records since 2015 (Fig. 5).

We show that increases in annual-scale AMP intensity in recent decades are driven, in part, by the presence of positive trends in SMP intensity during JJA across the interior WUS. For example, although domain-median decreases in SMP intensity of 11-16% are observed across the subdaily aggregations during 1980-2024, there are broad intensity increases in the more recent 2000-2024 period (Fig. 6). Notably, this result contrasts with the findings of Barbero et al. (2017) who reported minimal changes in JJA SMP_{1HR} intensity using data through 2011. Furthermore, our results suggest that the inclusion of the most recent 13 years of data allows for detection of recent SMP_{1HR} intensification during JJA in the WUS not apparent in earlier studies.

We further link this recent intensification with shifts in JJA thermodynamic environments. Over the full 1980-2024 period, TCWV, DEW_{2M}, and CAPE have generally decreased across the WUS and, given their widespread positive correlation with SMP_{1HR} intensity (Fig. 9), thus trended toward less favorable conditions for extreme subdaily precipitation. Over 2000-2024, however, widespread TCWV increases are apparent with some regional increases in DEW_{2M} and CAPE across the interior WUS (Fig. 10), and TCWV increases are more widespread in other seasons, as well, compared to the full 1980-2024 period. We further point out that increases in TCWV may also portend an increasing risk of subdaily precipitation extremes when the right meteorological ingredients align, including in areas that have not recently experienced increased AMP or SMP intensity (e.g., the Northwest).

4.2. Implications

Evidence of recent intensification of annual maximum subdaily precipitation in the WUS presented herein is consistent with physical expectations from a warming climate and increased moisture-carrying capacity of the atmosphere, and highlights the potential for further intensification of these extremes in the near future (Fowler et al., 2021; Nanditha et al., 2025; Prein et al., 2017; Zhang et al., 2017). Indeed, the observed 7% intensification of JJA SMP_{1HR} events between 2000 and 2024 reported in this study – a period over which the WUS warmed by ~0.93 °C during this season (NCEI, 2025) – although not statistically significant, is comparable to the C-C scaling relationship with a warming atmosphere (observed ~7.5% per °C). While the unusual number of period-of-record maximum 1-hr precipitation events since 2015 could be due to stochastic processes or natural climate variability, it may also suggest that these extremes have indeed begun to increase in the WUS due to anthropogenic climate change.

Collectively, our results imply that the juxtaposition of multidecadal climate signals – including the late 20th century wet period immediately followed by the early 21st century "megadrought" (Cook et al., 2025; Williams et al., 2022) – likely masked signals of anthropogenic intensification of subdaily precipitation extremes over the last four decades, muting intensity trends over the full 1980-2024 period (similar to the argument made by Bass et al. (2022)). These signals have likely only become more apparent with the most recent observational data, indicating that an "unmasking" may now be underway, at least for subdaily precipitation extremes. This possible early detection of increases in WUS annual maximum subdaily precipitation in recent decades – representing a "reversal" from longer-term decreasing trends – along with an increase in period-of-record maximum precipitation extremes, has potentially important implications for water and flood management as well as disaster preparedness. Thus, from a water and flood risk management perspective, it is important to recognize that short-duration precipitation extremes may evolve differently than longer daily-to-multiday ones (Hoerling et al., 2016; Williams et al., 2024), and that muted or absent long-term trends in average conditions may be unrepresentative of changes in the most extreme precipitation events (Swain et al., 2018).

4.3. Concluding remarks

Given the considerable uncertainties involved in analyzing subdaily precipitation across spatial scales, continued assessment with high quality gauge-based data and convection-permitting atmospheric modeling will be critical for understanding and projecting future changes in subdaily precipitation extremes. This is especially true in orographically-favored or otherwise remote locations in topographically complex portions of the WUS that in many cases remain ungauged. Potential shifts in the frequency of large-scale atmospheric patterns conducive to extreme precipitation could also modulate future trends in subdaily precipitation extremes, warranting further study over this region (Bass et al., 2022; Dallan et al., 2024; Pfahl et al., 2017). These shifts could result from either anthropogenic forcing or long-term variability in ENSO and PDO phases that could impact JJA SMP intensity despite a lack of robust correlations at the scale of individual seasons (Fig. 8), due to, for example, changes in precipitation recycling from abnormally wet or dry soils (Skinner et al., 2023). Finally, given the susceptibility of many fast-responding watersheds and urban areas to rapid inundation by flash flooding and debris flows posed by intense, short-duration rainfall – particularly in and near the growing expanse affected by large and high-intensity wildfire (Cunningham et al., 2025) where surface runoff is maximized (Staley et al., 2017; Thomas et al., 2024; Touma et al., 2022) – our results highlight that intensifying subdaily precipitation extremes in the WUS should be an urgent consideration in ongoing adaptation and planning efforts.

CRediT authorship contribution statement

Dmitri A. Kalashnikov: Conceptualization, Data curation, Formal analysis, Funding acquisition, Investigation, Methodology, Software, Validation, Visualization, Writing – original draft, Writing – review & editing. **John T. Abatzoglou:** Conceptualization, Methodology, Project administration, Resources, Software, Supervision, Writing – review & editing. **Daniel L. Swain:** Conceptualization, Methodology, Writing – review & editing.

Declaration of competing interest

The authors declare the following financial interests/personal relationships which may be considered as potential competing interests: Dmitri Kalashnikov reports financial support was provided by National Science Foundation. If there are other authors, they declare that they have no known competing financial interests or personal relationships that could have appeared to influence the work reported in this paper.

Acknowledgments

We thank Daryl Herzmann and the Iowa Environmental Mesonet at Iowa State University for archiving and providing access to the ASOS data, and the National Centers for Environmental Information for providing access to the HPD and GHCNd data. DAK was supported by

NSF award AGS-PRF #2403765. JTA was partially supported by USDA National Institute of Food and Agriculture Awards #2021-69012-35916 and 2021-67021-35344.

Appendix A. Supplementary data

Supplementary data to this article can be found online at https://doi.org/10.1016/j.wace.2026.100915.

Data availability

Code to create the figures can be accessed at the following GitHub repository: https://github.com/dmitri1357/subdaily_precipitation_extremes. Station precipitation datasets used in this study are openly available at https://mesonet.agron.iastate.edu/request/download.phtml (ASOS), https://www.ncei.noaa.gov/access/metadata/landing-page/bin/iso?id=gov.noaa.ncdc:C00988 (HPD), and https://www.ncei.noaa.gov/products/land-based-station/global-historical-climatology-network-daily (GHCNd). ERA5 data can be accessed at: https://cds.climate.copernicus.eu/datasets/reanalysis-era5-single-levels?tab=download. NLDN lightning data were sourced from the National Centers for Environmental Information Severe Weather Data Inventory (https://www.ncei.noaa.gov/pub/data/swdi/database-csv/v2/). CPC data links for climate variability indices are as follows: RONI (https://www.cpc.ncep.noaa.gov/products/analysis_monitoring/enso/roni/), AO (https://www.cpc.ncep.noaa.gov/products/precip/CWlink/daily_ao_index/ao.shtml). NCEI PDO data were sourced from https://www.ncei.noaa.gov/access/monitoring/pdo/. Elevation data are from the ETOPO Global Relief Model (ETOPO, 2022) at 30 arc-second resolution ("Bedrock elevation geotiff") sourced from the NCEI: https://www.ncei.noaa.gov/products/etopo-global-relief-model).

References

Abatzoglou, J.T., Barbero, R., 2014. Observed and projected changes in absolute temperature records across the contiguous United States. Geophys. Res. Lett. 41 (18), 6501–6508. https://doi.org/10.1002/2014GL061441.

Adams, D.K., Comrie, A.C., 1997. The North American monsoon. Bull. Am. Meteorol. Soc. 78 (10), 2197–2213. https://doi.org/10.1175/1520-0477(1997)078<2197:TNAM>2.0.CO;2.

Ahmadalipour, A., Moradkhani, H., 2019. A data-driven analysis of flash flood hazard, fatalities, and damages over the CONUS during 1996–2017. J. Hydrol. 578, 124106. https://doi.org/10.1016/j.jhydrol.2019.124106.

Ali, H., Fowler, H.J., Lenderink, G., Lewis, E., Pritchard, D., 2021. Consistent large-scale response of hourly extreme precipitation to temperature variation over land. Geophys. Res. Lett. 48 (4). https://doi.org/10.1029/2020gl090317 e2020GL090317.

Allen, M.R., Ingram, W.J., 2002. Constraints on future changes in climate and the hydrologic cycle. Nature 419, 224–232.

Ashley, S.T., Ashley, W.S., 2008. Flood fatalities in the United States. J. Appl. Meteorol. Climatol. 47 (3), 805–818. https://doi.org/10.1175/2007JAMC1611.1.

Barbero, R., Fowler, H.J., Lenderink, G., Blenkinsop, S., 2017. Is the intensification of precipitation extremes with global warming better detected at hourly than daily resolutions? Geophys. Res. Lett. 44 (2), 974–983. https://doi.org/10.1002/2016GL071917.

Barbero, R., Westra, S., Lenderink, G., Fowler, H.J., 2018. Temperature-extreme precipitation scaling: a two-way causality? Int. J. Climatol. 38 (S1), e1274–e1279. https://doi.org/10.1002/joc.5370.

Barlow, M., Nigam, S., Berbery, E.H., 1998. Evolution of the North American monsoon system. J. Clim. 11 (9), 2238–2257. https://doi.org/10.1175/1520-0442(1998)011<2238:EOTNAM>2.0.CO;2.

Bass, B., Norris, J., Thackeray, C., Hall, A., 2022. Natural variability has concealed increases in western US flood hazard since the 1970s. Geophys. Res. Lett. 49 (7). https://doi.org/10.1029/2021GL097706 e2021GL097706.

Brooks, H.E., Stensrud, D.J., 2000. Climatology of heavy rain events in the United States from hourly precipitation observations. Mon. Weather Rev. 128 (4), 1194–1201. https://doi.org/10.1175/1520-0493(2000)128<1194:COHREI>2.0.CO;2.

Cannon, A.J., Jeong, D.-I., Yau, K.-H., 2024. Updated observations provide stronger evidence for increases in subhourly to hourly extreme rainfall in Canada. J. Clim. 37 (12), 3393–3411. https://doi.org/10.1175/JCLI-D-23-0501.1.

Center for Western Weather and Water Extremes (CW3E), 2024. CW3E Analysis: Heavy Rain in San Diego, CA (22 Jan 2024). Center for Western Weather and Water Extremes, Scripps Institution of Oceanography, University of California, San Diego. Available at: https://cw3e.ucsd.edu/wp-content/uploads/2024/01/20240131_SD_Summary/CW3E_AR_Summary_20240122.pdf. (Accessed 25 August 2025).

Cook, B.I., Williams, A.P., Smerdon, J.E., Marvel, K., Seager, R., 2025. Megapluvials in Southwestern North America. AGU Adv. 6 (2). https://doi.org/10.1029/2024av001508 e2024AV001508.

Court, A., 1960. Reliability of hourly precipitation data. J. Geophys. Res. 65 (12), 4017–4024. https://doi.org/10.1029/JZ065i012p04017.

Cummins, K.L., Murphy, M.J., 2009. An overview of lightning locating systems: history, techniques, and data uses, with an in-depth look at the U.S. NLDN. IEEE Trans. Electromagn C. 51 (3), 499–518. https://doi.org/10.1109/TEMC.2009.2023450.

Cunningham, C.X., Abatzoglou, J.T., Ellis, T.M., Williamson, G.J., Bowman, D.M.J.S., 2025. Wildfires will intensify in the wildland-urban interface under near-term warming. Commun. Earth Environ. 6, 542. https://doi.org/10.1038/s43427-025-02475-y.

Dallan, E., Marra, F., Fosser, G., Marani, M., Borga, M., 2024. Dynamical factors heavily modulate the future increase of sub-daily extreme precipitation in the alpine-mediterranean region. Earths Future 12 (12). https://doi.org/10.1029/2024EF005185 e2024EF005185.

Fowler, H.J., Lenderink, G., Prein, A.F., Westra, S., Allan, R.P., Ban, N., et al., 2021. Anthropogenic intensification of short-duration rainfall extremes. Nat. Rev. Earth Environ. 2, 107–122.

Graff, A., 2023. Oxnard gets 3 inches of rain in an hour as storm wallops Southern California, SFGATE, 21 December. https://www.sfgate.com/bayarea/article/ventura-county-storm-flooding-southern-california-18568176.php. (Accessed 25 August 2025).

Groisman, P.Y., Knight, R.W., Karl, T.R., 2012. Changes in intense precipitation over the central United States. J. Hydrometeorol. 13 (1), 47–66. https://doi.org/10.1175/JHM-D-11-039.1.

Groisman, P.Y., Legates, D.R., 1994. The accuracy of United States precipitation data. Bull. Am. Meteorol. Soc. 75 (2), 215–227. https://doi.org/10.1175/1520-0477(1994)075<0215:TAOUSP>2.0.CO;2.

Hersbach, H., Bell, B., Berrisford, P., Hirahara, S., Horányi, A., Muñoz-Sabater, J., et al., 2020. The ERA5 global reanalysis. Q. J. R. Meteorol. Soc. 146 (730), 1999–2049. https://doi.org/10.1002/qj.3803.

Hoerling, M., Eischeid, J., Perlwitz, J., Quan, X.-W., Wolter, K., Cheng, L., 2016. Characterizing recent trends in U.S. heavy precipitation. J. Clim. 29 (7), 2313–2332. https://doi.org/10.1175/JCLI-D-15-0441.1.

Horel, J.D., Powell, J.T., 2024. Analysis and prediction of summer rainfall over southwestern Utah. Weather Forecast. 39 (7), 1007–1021. https://doi.org/10.1175/WAF-D-24-0018.1.

Huang, X., Swain, D.L., Hall, A.D., 2020. Future precipitation increase from very high resolution ensemble downscaling of extreme atmospheric river storms in California. Sci. Adv. 6 (29). https://doi.org/10.1126/sciadv.aba1323 aba1323.

James, E.P., Schumacher, R.S., 2024. Precipitation proxies for flash flooding: a seven-year analysis over the contiguous United States. J. Hydrometeorol. 25 (9), 1323–1344. https://doi.org/10.1175/JHM-D-23-0203.1.

Kendon, E.J., Fischer, E.M., Short, C.J., 2023. Variability conceals emerging trend in 100yr projections of UK local hourly rainfall extremes. Nat. Commun. 14, 1133. https://doi.org/10.1038/s41467-023-36499-9.

Lawrimore, J.H., Wuertz, D., Wilson, A., Stevens, S., Menne, M., Korzeniewski, B., et al., 2020. Quality control and processing of cooperative observer program hourly precipitation data. J. Hydrometeorol. 21 (8), 1811–1825. https://doi.org/10.1175/JHM-D-19-0300.1.

Lenderink, G., Barbero, R., Loriaux, J.M., Fowler, H.J., 2017. Super-Clausius–Clapeyron scaling of extreme hourly convective precipitation and its relation to large-scale atmospheric conditions. J. Clim. 30 (15), 6037–6052. https://doi.org/10.1175/JCLI-D-16-0808.1.

Lewis, E., Fowler, H., Alexander, L., Dunn, R., McClean, F., Barbero, R., et al., 2019. GSDR: a global sub-daily rainfall dataset. J. Clim. 32 (15), 4715–4729. https://doi.org/10.1175/JCLI-D-18-0143.1.

Lewis, E., Pritchard, D., Villalobos-Herrera, R., Blenkinsop, S., McClean, F., Guerreiro, S., et al., 2021. Quality control of a global hourly rainfall dataset. Environ. Model. Softw. 144, 105169. https://doi.org/10.1016/j.envsoft.2021.105169.

Li, X.-F., Blenkinsop, S., Barbero, R., Yu, J., Lewis, E., Lenderink, G., et al., 2020. Global distribution of the intensity and frequency of hourly precipitation and their responses to ENSO. Clim. Dyn. 54, 4823–4839. https://doi.org/10.1007/s00382-020-05258-7.

Li, L., Li, Z., 2023. Potential intensification of hourly precipitation extremes in Western Canada: a comprehensive understanding of precipitation-temperature scaling. Atmos. Res. 295, 106979. https://doi.org/10.1016/j.atmosres.2023.106979.

Liner, S., Ryoo, J.-M., Chiao, S., 2022. On the relationship of arctic oscillation with atmospheric rivers and snowpack in the western United States using long-term multi-platform dataset. Water 14 (15), 2392. https://doi.org/10.3390/w14152392.

Maddox, R.A., Canova, F., Hoxit, L.R., 1980. Meteorological characteristics of flash flood events over the western United States. Mon. Weather Rev. 108 (11), 1866–1877. https://doi.org/10.1175/1520-0493(1980)108<1866:MCOFFE>2.0.CO;2.

Mascaro, G., Farris, S., Deidda, R., 2025. Evidence of emerging increasing trends in observed subdaily heavy precipitation frequency in the United States. Geophys. Res. Lett. 52 (12). https://doi.org/10.1029/2024gl114292 e2024GL114292.

McCabe-Glynn, S., Johnson, K.R., Strong, C., Zou, Y., Yu, J.-Y., Sellars, S., Welker, J.M., 2016. Isotopic signature of extreme precipitation events in the western U.S. and associated phases of arctic and tropical climate modes. J. Geophys. Res. Atmos. 121 (15), 8913–8924. https://doi.org/10.1002/2016JD025524.

McKinnon, K.A., Deser, C., 2021. The inherent uncertainty of precipitation variability, trends, and extremes due to internal variability, with implications for Western US

water resources. J. Clim. 34 (24), 9605–9622. https://doi.org/10.1175/JCLI-D-21-0251.1.
Mock, C.J., 1996. Climatic controls and spatial variations of precipitation in the western United States. J. Clim. 9 (5), 1111–1125. https://doi.org/10.1175/1520-0442(1996)009<1111:CCASVO>2.0.CO;2.
Nanditha, Villarini, G., Misra, S., White, K., 2025. Regional variability in the projected changes in sub-daily precipitation IDF curves across the contiguous United States. Environ. Res. Lett. 20 (9), 094006. https://doi.org/10.1088/1748-9326/adf07d.
National Centers for Environmental Information (NCEI), 2025. Regional time series, climate at a glance regional time series. Nat. Cent. Environ. Inform. Available at: https://www.ncei.noaa.gov/access/monitoring/climate-at-a-glance/regional/time-series/124/tavg/3/8/2000-2024?trend=true&trend_base=10&begtrendyear=2000&endtrendyear=2024. (Accessed 1 September 2025).
National Park Service (NPS), 2022. DEVA Deluge 2022, Death Valley National Park. National Park Service. Available at: https://www.nps.gov/deva/learn/nature/deva-deluge-2022.htm. (Accessed 25 August 2025).
National Weather Service (NWS), 2023. Review of the 2022 Monsoon Across the Southwest U.S. National Weather Service, Phoenix, AZ. Available at: https://www.weather.gov/psr/2022MonsoonReview. (Accessed 25 August 2025).
National Weather Service (NWS), 2026. ENSO effect on our winter weather, national weather service, Tampa Bay area, FL. https://www.weather.gov/tbw/ENSOWinter. (Accessed 14 May 2026).
Oakley, N.S., Cannon, F., Munroe, R., Lancaster, J.T., Gomberg, D., Ralph, F.M., 2018. Brief communication: meteorological and climatological conditions associated with the 9 January 2018 post-fire debris flows in montecito and carpinteria California, USA. Nat. Hazards Earth Syst. Sci. 18 (11), 3037–3043. https://doi.org/10.5194/nhess-18-3037-2018.
Papalexiou, S.M., AghaKouchak, A., Foufoula-Georgiou, E., 2018. A diagnostic framework for understanding climatology of tails of hourly precipitation extremes in the United States. Water Resour. Res. 54 (9), 6725–6738. https://doi.org/10.1029/2018WR022732.
Patricola, C.M., O'Brien, J.P., Risser, M.D., Rhoades, A.M., O'Brien, T.A., Ullrich, P.A., et al., 2020. Maximizing ENSO as a source of western US hydroclimate predictability. Clim. Dyn. 54, 351–372. https://doi.org/10.1007/s00382-019-05004-8.
Pettitt, A.N., 1979. A non-parametric approach to the change-point problem. J. R. Stat. Soc. C-Appl. Stat. 28 (2), 126–135. https://doi.org/10.2307/2346729.
Pfahl, S., O'Gorman, P.A., Fischer, E.M., 2017. Understanding the regional pattern of projected future changes in extreme precipitation. Nat. Clim. Change 7, 423–427. https://doi.org/10.1038/NCLIMATE3287.
Prein, A.F., Rasmussen, R.M., Ikeda, K., Liu, C., Clark, M.P., Holland, G.J., 2017. The future intensification of hourly precipitation extremes. Nat. Clim. Change 7, 48–52. https://doi.org/10.1038/NCLIMATE3168.
Pritchard, D., Lewis, E., Blenkinsop, S., Patino Velasquez, L., Whitford, A., Fowler, H.J., 2023. An observation-based dataset of global sub-daily precipitation indices (GSDR-I). Sci. Data 10, 393. https://doi.org/10.1038/s41597-023-02238-4.
Ralph, F.M., Dettinger, M., White, A., Reynolds, D., Cayan, D., Schneider, T., et al., 2014. A vision for future observations for western U.S. extreme precipitation and flooding. J. Contemp. Water Resour. Educ. 153 (1), 16–32. https://doi.org/10.1111/j.1936-704X.2014.03176.x.
Reinhart, B.J., 2024. Hurricane Hilary (EP092023). National Hurricane Center Tropical Cyclone Report. Available at: https://www.nhc.noaa.gov/data/tcr/EP092023_Hilary.pdf. (Accessed 17 November 2025).
Simpson, I.R., McKinnon, K.A., Kennedy, D., Lawrence, D.M., Lehner, F., Seager, R., 2024. Observed humidity trends in dry regions contradict climate models. Proc. Natl. Acad. Sci. U. S. A 121 (1), e2302480120. https://doi.org/10.1073/pnas.2302480120.
Skinner, C.B., Harrington, T.S., Barlow, M., Agel, L., 2023. The contribution of precipitation recycling to North American wet and dry precipitation extremes. Environ. Res.: Clim. Past 2 (4), 045010. https://doi.org/10.1088/2752-5295/acffea.
Smith, J.A., Baeck, M.L., Yang, L., Signell, J., Morin, E., Goodrich, D.C., 2019. The paroxysmal precipitation of the desert: flash floods in the southwestern United States. Water Resour. Res. 55 (12), 10218–10247. https://doi.org/10.1029/2019WR025480.
Smith, J.A., Cox, A.A., Baeck, M.L., Yang, L., Bates, P., 2018. Strange floods: the upper tail of flood peaks in the United States. Water Resour. Res. 54 (9), 6510–6542. https://doi.org/10.1029/2018WR022539.
Staley, D.M., Negri, J.A., Kean, J.W., Laber, J.L., Tillery, A.C., Youberg, A.M., 2017. Prediction of spatially explicit rainfall intensity–duration thresholds for post-fire debris-flow generation in the western United States. Geomorphology 278, 149–162. https://doi.org/10.1016/j.geomorph.2016.10.019.
Swain, D.L., Langenbrunner, B., Neelin, J.D., Hall, A., 2018. Increasing precipitation volatility in twenty-first century California. Nat. Clim. Change 8, 427–433. https://doi.org/10.1038/s41558-018-0140-y.
Thomas, M.A., Michaelis, A.C., Oakley, N.S., Kean, J.W., Gensini, V.A., Ashley, W.S., 2024. Rainfall intensification amplifies exposure of American Southwest to conditions that trigger postfire debris flows. NPJ Nat. Hazards 1, 14. https://doi.org/10.1038/s44304-024-00017-8.
Touma, D., Stevenson, S., Swain, D.L., Singh, D., Kalashnikov, D.A., Huang, X., 2022. Climate change increases risk of extreme rainfall following wildfire in the western United States. Sci. Adv. 8 (13). https://doi.org/10.1126/sciadv.abm0320 eabm0320.
Trenberth, K.E., Dai, A., Rasmussen, R.M., Parsons, D.B., 2003. The changing character of precipitation. Bull. Am. Meteorol. Soc. 84 (9), 1205–1218. https://doi.org/10.1175/BAMS-84-9-1205.
Tukey, 1977. Exploratory Data Analysis. Pearson.
van der Drift, R.J., O'Gorman, P.A., 2025. Dependence of convective precipitation extremes on near-surface relative humidity. J. Clim. 38 (21), 6207–6225. https://doi.org/10.1175/JCLI-D-24-0738.1.
Wallis, J.R., Schaefer, M.G., Barker, B.L., Taylor, G.H., 2007. Regional precipitation-frequency analysis and spatial mapping for 24-hour and 2-hour durations for Washington state. Hydrol. Earth Syst. Sci. 11 (1), 415–442. https://doi.org/10.5194/hess-11-415-2007.
Westra, S., Alexander, L.V., Zwiers, F.W., 2013. Global increasing trends in annual maximum daily precipitation. J. Clim. 26 (11), 3904–3918. https://doi.org/10.1175/JCLI-D-12-00502.1.
Williams, A.P., Cook, B.I., Smerdon, J.E., 2022. Brief communication: rapid intensification of the emerging Southwestern North American megadrought in 2020-2021. Nat. Clim. Change 12, 232–234.
Williams, A.P., McKinnon, K.A., Anchukaitis, K.J., Gershunov, A., Varuolo-Clarke, A.M., Clemesha, R.E.S., Liu, H., 2024. Anthropogenic intensification of cool-season precipitation is not yet detectable across the western United States. J. Geophys. Res. Atmos. 129 (12). https://doi.org/10.1029/2023jd040537 e2023JD040537.
Wood, R.R., Ludwig, R., 2020. Analyzing internal variability and forced response of subdaily and daily extreme precipitation over Europe. Geophys. Res. Lett. 47 (17). https://doi.org/10.1029/2020gl089300 e2020GL089300.
Zhang, W., Villarini, G., Scoccimarro, E., Vecchi, G.A., 2017. Stronger influences of increased CO_2 on subdaily precipitation extremes than at the daily scale. Geophys. Res. Lett. 44 (14), 7464–7471. https://doi.org/10.1002/2017GL074024.